Arbitrary Prescribed Flat Wideband Group Delay Absorptive Microstrip Bandpass Filters

Girdhari Chaudhary, *Member, IEEE*, and Yongchae Jeong, *Senior Member, IEEE*

***Abstract*— This article demonstrates the design of microstrip line symmetrical all-band absorptive bandpass filters (BPFs) with arbitrarily prescribed wideband flat group delay (GD) characteristics. The proposed BPFs consist of coupled line sections with series resistor connected stubs (short-circuited quarter-wavelength or open-circuited half-wavelength stubs). Analytical design equations are derived to obtain circuit parameters for arbitrarily prescribed flat GD characteristics. A detailed analysis shows that the absorptive sections (series resistor connected stubs) not only eliminate out-of-band reflections, but also determine the passband GD flatness characteristics. The proposed absorptive BPFs with arbitrarily prescribed flat GD can be easily extended to a higher order by cascading the first-order symmetrical quasi-absorptive BPF. For experimental validation, first- and second-order quasi-absorptive BPFs were designed with arbitrarily prescribed GD of 1.75 and 3.40 ns, respectively, and measurements were taken at a center frequency of 3.5 GHz. The results of the measurement are in good agreement with the predictions obtained through theoretical methods and simulation.**

***Index Terms*— Absorptive bandpass filter (BPF), circulator, coupled line, microstrip line filter, wideband flat group delay (GD).**

I. Introduction

MULTIFUNCTIONAL, high-performance bandpass filters (BPFs) are in high demand for next-generation wireless communication systems. In recent years, absorptive or reflectionless RF BPF has become attractive to prevent interblock signal interference from unwanted RF-signal-power reflections and improve the stability of adjacent RF active circuits in RF front-end chains [1]. Conventional BPF topologies have a reflective nature in the stopband, which alleviates the need for nonreciprocal components that are bulky and difficult to integrate (e.g., isolators and circulators) in a complete RF system to avoid the unwanted RF-signal power reflections. Contrary to conventional reflection BPFs, absorptive or reflectionless filters dissipate inside themselves the nontransmitted input-signal energy in the stopband regions instead of reflecting it back to the source, which results in a more robust RF front-end chain by avoiding the creation of RF signal-power reflections without the need for passive/active nonreciprocal components. In addition, microwave filters with prescribed group delay (GD) response with respect to frequency have various applications in communication, real-time analog radio-signal processing (R-ASP), RF self-interference cancellation in-band full duplex radio, and signal cancellation in feed-forward amplifier [2]–[4]. Moreover, arbitrarily prescribed flat GD BPFs play important role in designing magnet-free nonreciprocal components, such as isolators, circulators, and nonreciprocal BPFs [5]–[7].

In recent years, absorptive or reflectionless BPFs based on different approaches and topologies have been investigated in the literature [8]–[27]. Absorptive BPFs are realized using a broadband coupler and a Wilkinson power divider, which are arranged in a two-branch structure, as reported in [8]. Reflectionless BPFs were presented by exploiting theoretically perfect matched circuits in [9]–[12]. In [13], first-order input-reflectionless BPF was developed by employing lumped-elements based on input-matching sections with resistive elements. In [14]–[16], absorptive filters were realized by using a complementary-duplexer architecture consisting of main and auxiliary channels with the opposite filtering functions. One-port absorptive multiband BPF [17] and filtering power divider [18] were realized by using a complementary susceptance cancellation method. Similarly, two-port absorptive filters could be realized by adding one more channel at the output port [19], [20].

One-port absorption or symmetrical two-port absorption for bandstop filters was realized by using low-Q lossy resonators in [21]–[24]. Similarly, a distributed quasi-absorptive BPF was presented in [25] by using resistor-loaded lossy resonators as its first resonator to absorb reflection in only one side. Symmetrical quasi-absorptive BPFs were realized by using a complementary branch-line BPF and a bandstop filter [26]. Similarly, a higher order and symmetrical all-band quasi-absorptive BPF was realized using a bandpass section (reflective type coupled line filter) and absorptive section (a matched resistor in series with a short-circuited stub) in [27]. Although these BPF topologies feature reflectionless characteristics for input and output, they still suffer from an arbitrarily prescribed flat GD characteristic. In addition, conventional absorptive BPFs mainly focus on a frequency-dependent magnitude transfer response rather than a GD response.

In this article, we demonstrate an analytical design method for a microstrip line quasi-absorptive BPF with arbitrarily prescribed flat GD. The arbitrarily prescribed GD and bandpass

Manuscript received June 18, 2020; revised September 6, 2020 and November 2, 2020; accepted November 22, 2020. Date of publication December 14, 2020; date of current version February 4, 2021. This work was supported by the National Research Foundation (NRF) of Korea Grant funded by Korea Government (MSIT) under Grant 2020R1A2C2012057 and in part by Basic Science Research Program through the NRF of Korea, funded by Ministry of Education, under Grant 2019R1A6A1A09031717. *(Corresponding author: Yongchae Jeong.)*

The authors are with the Division of Electronic and Information Engineering, IT Convergence Research Center, Jeonbuk National University, Jeonju 54896, South Korea (e-mail: girdharic@jbnu.ac.kr; ycjeong@jbnu.ac.kr).

Color versions of one or more figures in this article are available at https://doi.org/10.1109/TMTT.2020.3041483.

Digital Object Identifier 10.1109/TMTT.2020.3041483

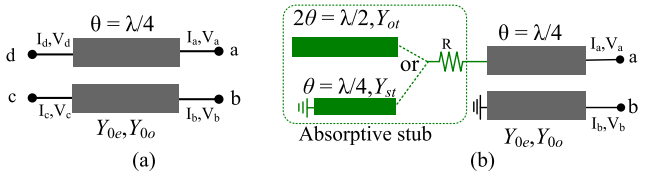

Fig. 1. (a) Four-port coupled line section and (b) two-port network with ports c and d are terminated with short-circuit and series R connected stubs, respectively.

response are realized by controlling a coupled line section and stubs. To achieve absorption at all frequencies, the absorptive stubs consisting of a series resistor and short-circuited quarter-wavelength or open-circuited half-wavelength stubs are connected at coupled sections. These stubs are open-circuit at a center frequency, whereas they appear as a matched load to the ground outside of the passband and contribute to the absorption of out-of-band signals. In addition, series resistors connected to the subs contribute to achieve a flat GD response in the passband. The proposed topologies are symmetrical all-band absorptive BPF, which can be easily extended to higher orders. For experimental validation, first- and second-order absorptive BPFs are designed and measured.

II. Design Theory

A. Building Block of Quasi-Absorptive BPF: Coupled Line With Series R Connected Stub

Fig. 1(a) shows a section of a $\lambda/4$ coupled line with four ports labeled as a, b, c, and d. The even- and odd-mode admittances (impedances) of the coupled line are denoted by $Y_{0e} = 1/Z_{0e}$ and $Y_{0o} = 1/Z_{0o}$, respectively. Assuming the coupling coefficient k is a free design variable, Y_{0e} is expressed in terms of k and Y_{0o} as

$$Y_{0e} = \frac{1-k}{1+k} Y_{0o}. \tag{1}$$

Fig. 1(b) shows a building block of the quasi-absorptive BPF. As shown in Fig. 1(b), the proposed two-port network is constructed by terminating port c and d of four-port coupled line with short-circuit and series resistor R connected stub (short-circuited $\lambda/4$ stub with characteristic admittance $Y_{ot} = 1/Z_{ot}$ or open-circuited $\lambda/2$ stub with characteristic admittance $Y_{st} = 1/Z_{st}$), respectively. For simplicity, the normalized frequency f/f_0 is used in the circuit analysis, where f and f_0 are the operating and passband center frequencies of the filter, respectively. The Y-parameters of the reduced two-port network shown in Fig. 1(b) are derived as

$$\begin{bmatrix} I_a \\ I_b \end{bmatrix} = \begin{bmatrix} Y_{aa} & Y_{ab} \\ Y_{ab} & Y_{bb} \end{bmatrix} \begin{bmatrix} V_a \\ V_b \end{bmatrix} \tag{2}$$

where

$$Y_{aa} = \frac{n_1 Y_{0o}^2}{m_1(1+k)^2} - j\frac{Y_{0o}}{1+k}\left\{\cot\frac{\pi f}{2f_0} - \frac{n_2 Y_{0o}}{m_1(1+k)}\right\} \tag{3a}$$

$$Y_{ab} = \frac{n_1 k Y_{0o}^2}{m_1(1+k)^2} - j\frac{kY_{0o}}{1+k}\left\{\cot\frac{\pi f}{2f_0} - \frac{n_2 Y_{0o}}{m_1(1+k)}\right\} \tag{3b}$$

$$Y_{bb} = \frac{n_1 k^2 Y_{0o}^2}{m_1(1+k)^2} - j\frac{Y_{0o}}{1+k}\left\{\cot\frac{\pi f}{2f_0} - \frac{n_2 k^2 Y_{0o}}{m_1(1+k)}\right\} \tag{3c}$$

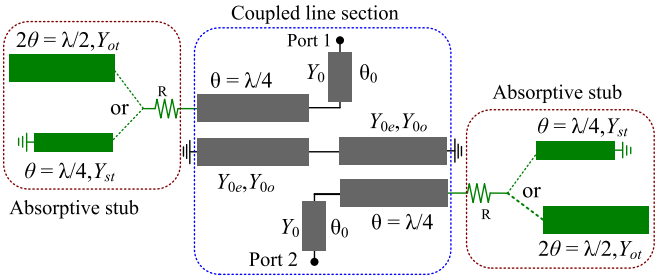

Fig. 2. Proposed structure of the first-order type-I quasi-absorptive BPF with arbitrarily prescribed GD.

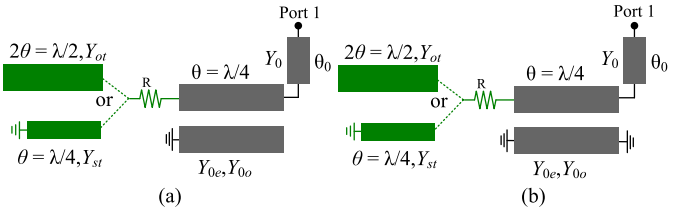

Fig. 3. Equivalent circuits of type-I absorptive BPF under (a) even-mode and (b) odd-mode.

$$m_1 = \left(\frac{1}{Z_{\lambda i}} + \frac{Y_{0o}}{1+k}\cot\frac{\pi f}{2f_0}\right)^2 + \frac{R^2 Y_{0o}^2}{Z_{\lambda i}^2(1+k)^2}\cot^2\frac{\pi f}{2f_0} \tag{3d}$$

$$n_1 = \frac{R}{Z_{\lambda i}^2}\csc^2\frac{\pi f}{2f_0} \tag{3e}$$

$$n_2 = \left\{\frac{1}{Z_{\lambda i}} + \frac{R^2 Y_{0o}}{Z_{\lambda i}^2(1+k)}\cot\frac{\pi f}{2f_0} + \frac{Y_{0o}}{1+k}\cot\frac{\pi f}{2f_0}\right\}\csc^2\frac{\pi f}{2f_0} \tag{3f}$$

$$Z_{\lambda i} = \begin{cases} -\dfrac{1}{Y_{ot}}\cot\dfrac{\pi f}{f_0} & \text{for open circuited } \dfrac{\lambda}{2}\text{stub} \\ \dfrac{1}{Y_{st}}\tan\dfrac{\pi f}{2f_0} & \text{for short-circuited } \dfrac{\lambda}{4}\text{stub.} \end{cases} \tag{3g}$$

B. Type-I: Arbitrarily Prescribed GD First-Order Quasi-Absorptive BPF With a Singly Loaded Absorptive Network

Fig. 2 shows the proposed structure of the first-order type-I quasi-absorptive BPF, which is constructed by connecting two back-to-back singly loaded quasi-absorptive coupled lines. To connect RF ports for measurement purpose, additional transmission lines (TLs) with characteristic impedance $Z_0 = 1/Y_0 = 50\ \Omega$ and electrical length θ_0 are added at input and output ports. As seen in Fig. 2, the proposed type-I absorptive BPF is symmetrical, which can be analyzed using an even- and odd-mode analysis. Fig. 3 shows the equivalent circuits of the proposed type-I absorptive BPF under even- and odd-mode excitations. Using Fig. 3, the even- and odd-mode admittances for the type-I filter can be written as

$$Y_{\text{Type-I\_even}} = Y_0\frac{Y_{aa}Y_{bb} - Y_{ab}^2 + jY_0Y_{bb}\tan(\theta_0 f/f_0)}{Y_0Y_{bb} + j\left(Y_{aa}Y_{bb} - Y_{ab}^2\right)\tan(\theta_0 f/f_0)} \tag{4a}$$

$$Y_{\text{Type-I\_odd}} = Y_0\frac{Y_{aa} + jY_0\tan(\theta_0 f/f_0)}{Y_o + jY_{aa}\tan(\theta_0 f/f_0)}. \tag{4b}$$

Using even- and odd-mode input admittances, the S-parameters of a type-I quasi-absorptive BPF can be

TABLE I
CALCULATED CIRCUIT PARAMETERS OF TYPE-I BPF WITH ARBITRARILY PRESCRIBED GD WITH $\theta_0 = 45°$ (REFER TO FIG. 4)

$\tau_{f=f_0}^{Type-I} \times f_0$	k (dB)	$Z_{0e}=1/Y_{0e}$ (Ω)	$Z_{0o}=1/Y_{0o}$ (Ω)	$Z_{ot}=1/Y_{ot}$ (Ω)	R (Ω)
6	-12.6	124.2038	77.0300	30	130
8	-14.4	139.4312	94.7995	30	160

expressed as

$$S_{11}^{\text{Type-I}} = S_{22}^{\text{Type-I}} = \frac{Y_0^2 - Y_{\text{Type-I-even}} Y_{\text{Type-I-odd}}}{\left(Y_0 + Y_{\text{Type-I-even}}\right)\left(Y_0 + Y_{\text{Type-I-odd}}\right)} \tag{5a}$$

$$S_{21}^{\text{Type-I}} = S_{12}^{\text{Type-I}} = \frac{\left(Y_{\text{Type-I-odd}} - Y_{\text{Type-I-even}}\right) Y_0}{\left(Y_0 + Y_{\text{Type-I-even}}\right)\left(Y_0 + Y_{\text{Type-I-odd}}\right)} \tag{5b}$$

where $Y_0 = 1/Z_0$ is a port admittance. Using the phase of $S_{21}^{\text{Type-I}}$, the GD of type-I BPF according to f can be calculated as

$$\tau|^{\text{Type-I}} = -\frac{1}{2\pi}\frac{d\angle S_{21}^{\text{Type-I}}}{df}. \tag{6}$$

To calculate circuit parameters with arbitrarily prescribed GD, (6) is further simplified at $f = f_0$

$$\tau|_{f=f_0}^{\text{Type-I}} = \frac{aY_{0o}^3 + Y_{0o}c + d}{4f_0 b Y_{0o}^2} + \frac{\theta_0}{\pi f_0} \tag{7}$$

where

$$a = \frac{1-k^2}{Y_0^2(1+k)^3}, \quad b = \frac{k^2}{Y_0(1+k)^2}, \quad c = \frac{k^2}{1+k} \tag{8a}$$

$$d = \begin{cases} k^2 Y_{\text{st}} = \dfrac{k^2}{Z_{\text{st}}} \text{ for short-circuited } \dfrac{\lambda}{4}\text{stub} \\ 2k^2 Y_{\text{ot}} = \dfrac{2k^2}{Z_{\text{ot}}} \text{ for open-circuited } \dfrac{\lambda}{2}\text{stub}. \end{cases} \tag{8b}$$

Based on the analytical analysis, arbitrarily specified flat GD and magnitude response can be obtained by selecting the appropriate Y_{0o} and k if Y_{st} or Y_{ot} are specified by the designer. Therefore, the solution of Y_{0o} in terms of specified GD at f_0, k, Y_{st}, or Y_{ot} can be found as

$$aY_{0o}^3 - 4f_0 b\left(\tau|_{f=f_0}^{\text{Type-I}} - \frac{\theta_0}{\pi f_0}\right)Y_{0o}^2 + Y_{0o}c + d = 0. \tag{9}$$

As noted from (9), Y_{0o} has three roots and one of these roots is the optimum circuit parameter of the proposed BPF with an arbitrarily prescribed GD.

For illustration purposes, Fig. 4(a) shows the magnitude/GD responses of type-I BPF with different arbitrarily prescribed GDs. Table I gives the calculated circuit parameters. As seen from Table I, a higher GD can be achieved by decreasing k and Y_{0o}. The proposed filter can provide three reflection zeros in passband either at real or imaginary frequencies. Moreover, the proposed BPF shows quasi-absorptive responses with a return loss better than 9.5 dB at all frequencies. The transmission coefficient roll-off characteristics improved with an increasing GD.

Fig. 4(b) shows the magnitude/GD responses according to different R values. When $R = 0\ \Omega$, the filter response is

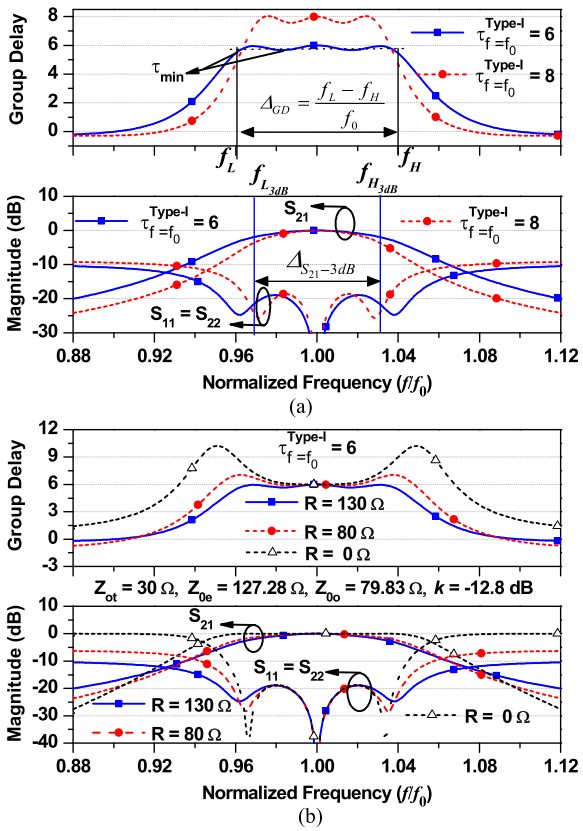

Fig. 4. Magnitude/GD responses of the first-order type-I BPF. (a) Different magnitude/GD. (b) Magnitude/GD according to R.

similar to a reflective-type Chebyshev filter. Similarly, the GD ripple can be minimized by increasing R without degrading the insertion loss (IL) at f_0. In addition, R also contributes to an improved absorption of out-of-band signals. In this work, the in-band GD ripple (τ_{ripple}) is defined as

$$\tau_{\text{ripple}} = \frac{\tau_{\max} - \tau_{\min}}{2} \tag{10}$$

where $\tau_{\max}$ and $\tau_{\min}$ are the maximum and minimum GD ripple within the passband (refer to Fig. 5), respectively. Similarly, the 3-dB passband and flat GD fractional bandwidth (FBW) of the proposed BPF can be calculated as

$$\Delta_{S_{21}-3\text{ dB}} = \frac{f_{H_{3\text{ dB}}} - f_{L_{3\text{ dB}}}}{f_0} = f\left(k, Y_{\text{ot}}, Y_{0o,}R\right) \tag{11a}$$

$$\Delta_{\text{GD}} = \frac{f_{\text{H}} - f_{\text{L}}}{f_0} = f\left(k, Y_{\text{ot}}, Y_{0o,}R\right) \tag{11b}$$

where $f_{L3\,\text{dB}}$, $f_{H3\,\text{dB}}$ are lower and upper cutoff frequencies of 3-dB passband, respectively (Fig. 4(a)). Similarly, f_{L} and f_{H} are the lower and upper cutoff frequencies in between which the GDs are equal to $\tau_{\min}$ within the passband as shown in Fig. 4(a). Once circuit parameters are determined for the specified GD at f_0, then minimum τ_{ripple}, 3-dB passband, and in-band GD FBWs are calculated by finding the cutoff frequencies using MATLAB.

Fig. 5(a) illustrates the magnitude/GD responses of the open-circuited $\lambda/2$ stub and short-circuited $\lambda/4$ stub for

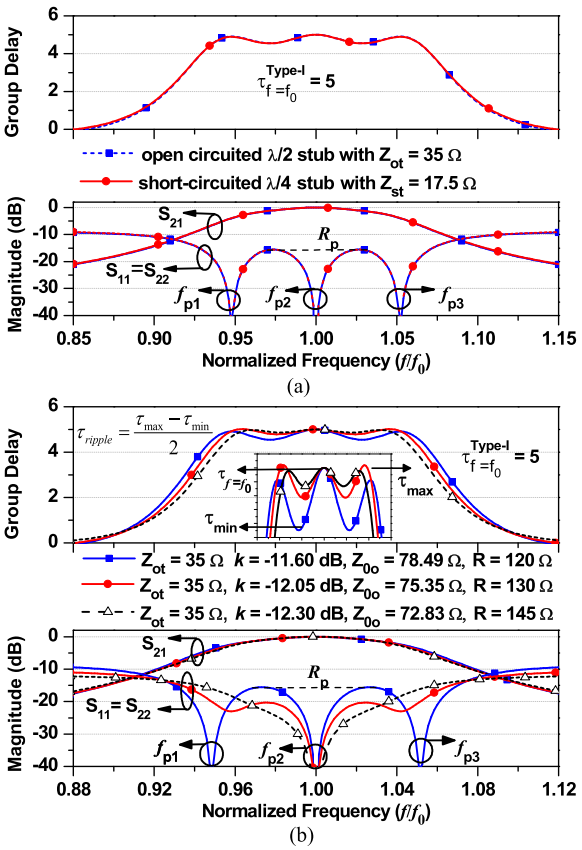

Fig. 5. Magnitude/GD response of first-order type-I BPF. (a) Comparison between $\lambda/2$ and $\lambda/4$ stub and (b) different k and $Y_{0o} = 1/Z_{0o}$.

TABLE II

CALCULATED CIRCUIT PARAMETERS OF THE TYPE-I BPF WITH A NORMALIZED GD $\tau_{f=f_0}^{\text{TYPE-I}} \times f_0 = 5$, $\theta_0 = 45°$, AND $Z_{ot} = 1/Y_{ot} = 35\ \Omega$ (REFER TO FIG. 5)

k (dB)	Z_{0e} $=1/Y_{0e}$ (Ω)	Z_{0o} $=1/Y_{0o}$ (Ω)	R (Ω)	$\Delta_{GD} = \frac{f_H - f_L}{f_0}$, $\Delta_{S_{21}-3dB}$ (%)	$\tau_{ripple} = \frac{\tau_{max}-\tau_{min}}{2}$
-11.30	132.26	75.65	120	10.35/9.63	0.22
-11.70	124.25	72.97	130	9.05/8.45	0.12
-12.0	117.01	70.03	145	8.78/8.42	0.06

comparison. As seen from Fig. 5(a), the same magnitude/GD responses can be achieved if $Z_{st} = Z_{ot}/2$.

Fig. 5(b) depicts the magnitude/GD responses of a BPF with different k, $Y_{0o} = 1/Z_{0o}$, and R. The calculated circuit parameters for Fig. 5 are shown in Table II. To facilitate a conclusive explanation, a few variables are labeled in Fig. 5 as R_p and f_{pi} ($i = 1, 2, 3$), which are defined as the maximum passband reflection and location of reflection zeros, respectively. As seen from Fig. 5, the in-band GD ripple is minimized by decreasing k and increasing R for a specified GD at $f = f_0$. Similarly, the calculated 3-dB passband and GD FBWs are shown in Table II.

As seen from Table II, 3-dB passband FBW is slightly smaller than in-band GD FBW. When the in-band GD ripple increases from 0.06 to 0.22, in-band GD and 3-dB passband

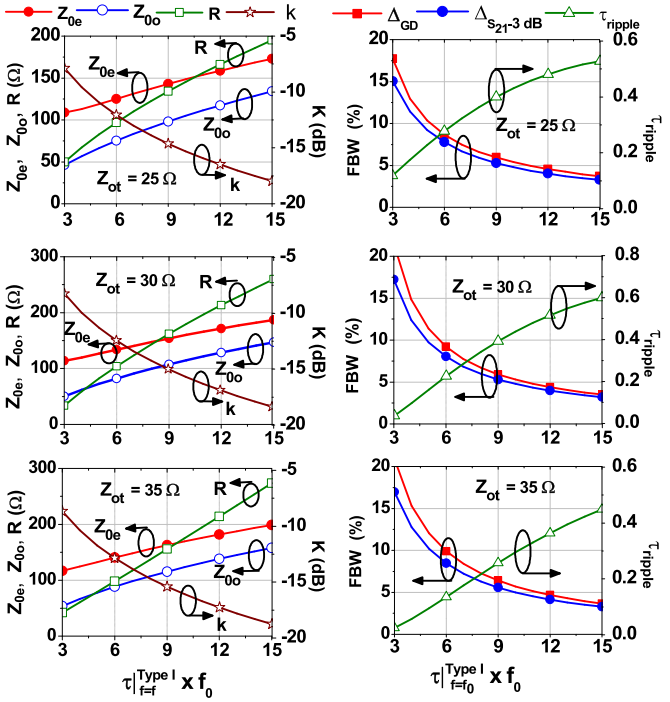

Fig. 6. Calculated circuit parameters of first-order type-I quasi-absorptive BPF with a passband maximum reflection (R_p) of -15 dB and $\theta_0 = 45°$.

FBWs increased from 8.78% to 10.20% and 8.42% to 9.28%, respectively. Also, the two reflection zeros f_{p1} and f_{p3} move toward f_{p2}, resulting in an improvement in R_p as well as 3-dB passband FBW.

Fig. 6 depicts the circuit parameters calculated for the type-I quasi-absorptive BPF with different GD as design graph. A higher GD can be achieved by decreasing k and increasing Z_{0o}. Meanwhile, the 3-dB passband and in-band GD FBWs decrease with an increasing GD. Therefore, a tradeoff exists among the in-band GD, 3-dB passband FBW, and GD. As observed from Fig. 6, Z_{0e} and Z_{0o} can decrease by reducing Z_{ot} for the same GD at $f = f_0$. In addition, a higher GD can be achieved by decreasing Z_{ot} with practical realizable coupled line Z_{0e} and Z_{0o} circuit parameters.

C. Type-II: Arbitrarily Prescribed GD First-Order Quasi-Absorptive BPF With a Double Absorptive Stub in Coupled Line Section

Fig. 7 shows the proposed structure of a first-order type-II arbitrarily prescribed GD absorptive BPF. The symmetrical structure of the type-II BPF is constructed by connecting absorptive stubs at the input and output port of the type-I BPF. As with type-I, the S-parameters of type-II BPF can be derived as follows using equivalent circuits under even- and odd-mode excitations, as shown in Fig. 8:

$$S_{11}^{\text{Type-II}} = S_{22}^{\text{Type-II}} = \frac{Y_0^2 - Y_{\text{Type-II-even}} Y_{\text{Type-II-odd}}}{\left(Y_0 + Y_{\text{Type-II-even}}\right)\left(Y_0 + Y_{\text{Type-II-odd}}\right)} \quad (12a)$$

$$S_{21}^{\text{Type-II}} = S_{12}^{\text{Type-II}} = \frac{\left(Y_{\text{Type-II-odd}} - Y_{\text{Type-II-even}}\right) Y_0}{\left(Y_0 + Y_{\text{Type-II-even}}\right)\left(Y_0 + Y_{\text{Type-II-odd}}\right)} \quad (12b)$$

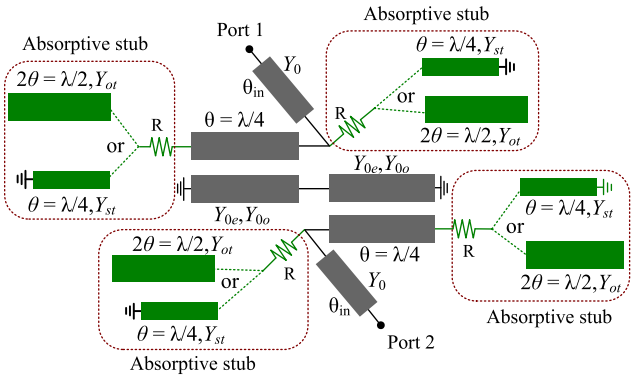

Fig. 7. Proposed structure of a type-II quasi-absorptive BPF with an arbitrarily prescribed GD.

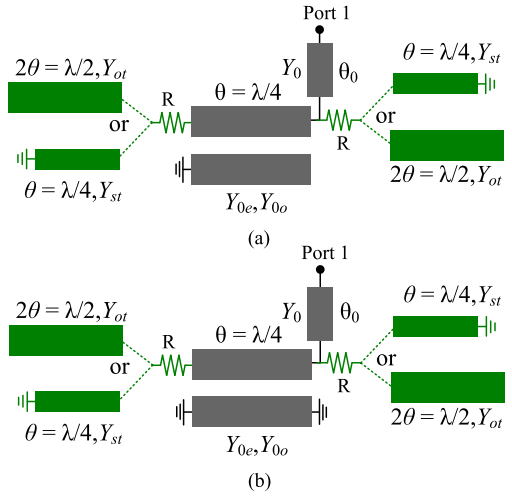

Fig. 8. Equivalent circuit of type-II absorptive BPF under (a) even-mode and (b) odd-mode excitations.

where

$$Y_{\text{Type-II\_even}} = Y_0 \frac{Y_m + jY_0 \tan(\theta_0 f/f_0)}{Y_0 + jY_m \tan(\theta_0 f/f_0)} \tag{13a}$$

$$Y_{\text{Type-II\_odd}} = Y_0 \frac{Y_n + jY_0 \tan(\theta_{\text{in}} f/f_0)}{Y_0 + jY_n \tan(\theta_{\text{in}} f/f_0)} \tag{13b}$$

$$Y_m = \frac{1}{R + jZ_{\lambda i}} + Y_{aa} - \frac{Y_{ab}^2}{Y_{bb}} \tag{13c}$$

$$Y_n = \frac{1}{R + jZ_{\lambda i}} + Y_{aa}. \tag{13d}$$

Using the phase of $S_{21}^{\text{Type-II}}$, the GD of a one-pole type-II BPF at $f = f_0$ can be derived

$$\tau|_{f=f_0}^{\text{Type-II}} = \frac{1}{4f_0}\left(\frac{aY_{0o}^3 + Y_{0o}c + d}{bY_{0o}^2} + \frac{e}{Y_0}\right) + \frac{\theta_0}{\pi f_0} \tag{14}$$

where

$$e = \begin{cases} Y_{\text{st}} = \dfrac{1}{Z_{\text{st}}} \text{for short-circuited } \dfrac{\lambda}{4} \text{stub} \\ 2Y_{\text{ot}} = \dfrac{2}{Z_{\text{ot}}} \text{for open-circuited } \dfrac{\lambda}{2} \text{stub}. \end{cases} \tag{15}$$

Equation (14) indicates that the GD of a first-order type-II BPF is higher than that for type-I due to the additional absorptive stubs at the input and output port. Using (14), the solution of Y_{0o} for the type-II BPF in terms of the specified GD at f_0, k, Y_{st}, or Y_{ot} can be obtained from

$$aY_{0o}^3 - 4f_0\left(\tau|_{f=f_0}^{\text{Type-II}} - \frac{e}{4Y_0 f_0} - \frac{\theta_0}{\pi f_0}\right)bY_{0o}^2 + Y_{0o}c + d = 0. \tag{16}$$

The required circuit parameters for the type-II BPF can be obtained by solving (16) by providing the values of GD, f_0, k, and $Y_{\text{ot}} = 1/Z_{\text{ot}}$. After obtaining $Y_{0o} = 1/Z_{0o}$, the $Y_{0e} = 1/Z_{0e}$ can also be found by using (1).

For illustration, Fig. 9 shows the S-parameter magnitude and GD responses of first-order type-I and type-II arbitrarily prescribed GD quasi-absorptive BPFs. The calculated circuit parameters are shown in Table III. As seen from Fig. 9, the 3-dB passband and in-band GD FBWs for the type-II BPF is wider than that for type-I for the same GD. The filter generates three reflection zeros in passband either at real or imaginary frequencies. In addition, the type-II BPF has an improved stopband reflection because of the additional absorptive stubs at the input and output ports, which contribute wider matching and transmission bandwidths as compared to type-I for the same GD.

Fig. 10 depicts the S-parameter magnitude and GD responses for the type-II for different arbitrary GD. As seen from Fig. 10, the BPF with a higher GD can be designed by decreasing k and increasing the odd-mode impedance of a coupled line when the characteristic impedance of the stub is fixed. With an increase in the GD, the 3-dB passband and GD FBW decreases, which results in improvements of the passband roll-off characteristics. Also, it is noted from Fig. 10

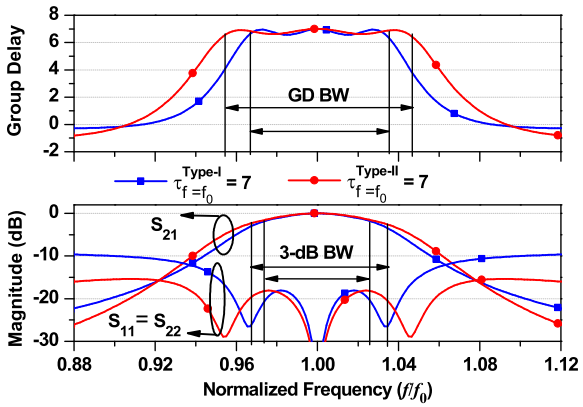

Fig. 9. Magnitude/GD responses comparison of first-order type-I and type-II BPF.

TABLE III
CALCULATED CIRCUIT PARAMETERS TYPE-I AND TYPE-II BPFS WITH $Z_{\text{ot}} = 1/Y_{\text{ot}} = 30\ \Omega$ AND $\theta_0 = 45°$ (REFER TO FIG. 9)

$\tau_{f=f_0} \times f_0$	Type-I BPF				Type-II BPF			
	Z_{0e} (Ω)	Z_{0o} (Ω)	R (Ω)	Δ_{GD} (%)	Z_{0e} (Ω)	Z_{0o} (Ω)	R (Ω)	Δ_{GD} (%)
7	133.2	86.7	135	7.10	134.2	81.78	90	9.36
$\Delta_{S_{21}-3dB}$	6.77%				7.62%			

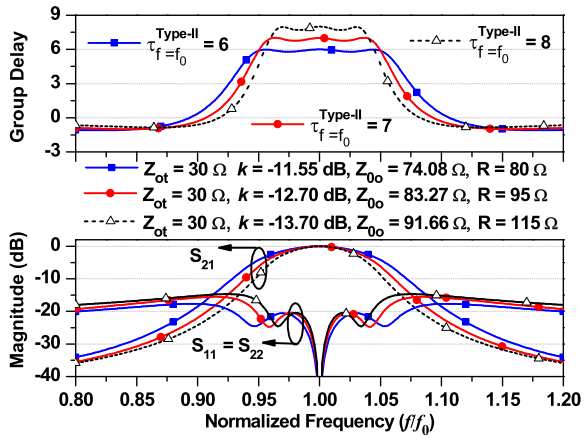

Fig. 10. Magnitude/GD responses of one-pole type-II BPF according to different k and $Y_{0o} = 1/Z_{0o}$ and $\theta_0 = 20°$.

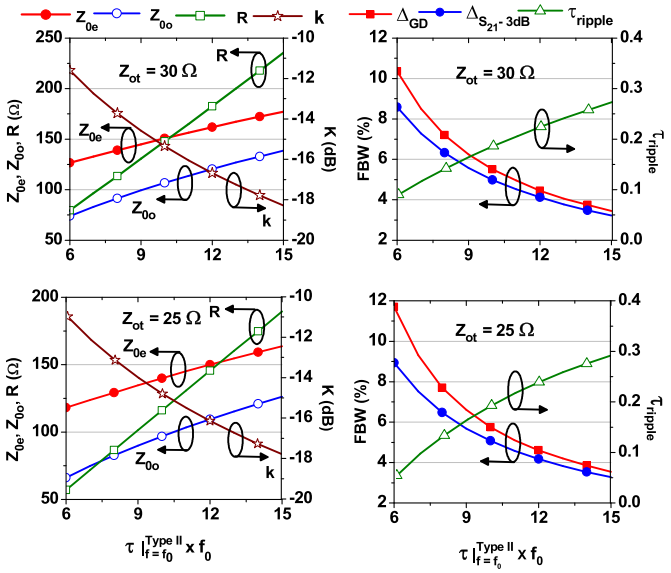

Fig. 11. Calculated circuit parameters of a first-order type-II BPF with a passband maximum reflection (R_p) of −20 dB and $\theta_0 = 45°$.

that reflection poles f_{p1} and f_{p3} move closer to f_{p2} when GD moves toward a higher value, resulting in a slight degradation in the maximum stopband reflection.

Fig. 11 depicts the calculated circuit parameters of a first-order type-II quasi-absorptive BPF with different GD and $Z_{ot} = 1/Y_{ot}$. As seen in Fig. 11, a higher GD can be achieved by increasing Z_{0o} and decreasing k. Similarly, 3-dB passband FBW is slightly smaller than in-band GD FBW and decreases with an increase in GD.

D. Extension to a Higher Order Quasi-Absorptive BPF With Arbitrarily Prescribed GD

The proposed quasi-absorptive BPFs with arbitrarily prescribed GD response can be extended to a higher order by cascading the one-pole BPF as shown in Fig. 12. For higher order, connecting line between one-pole quasi-absorptive BPF would be $2\theta_0$ (double of input–output transmission line). The

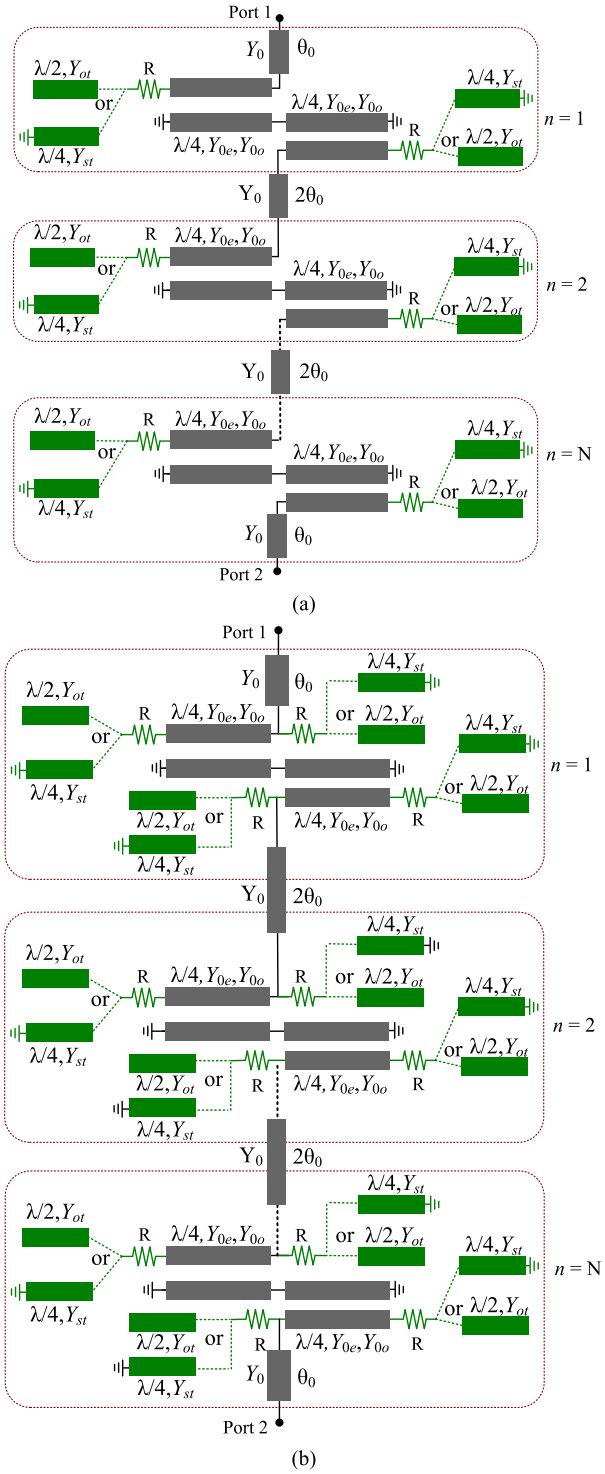

Fig. 12. Higher order quasi-absorptive BPFs with an arbitrarily prescribed GD. (a) Type-I. (b) Type-II.

overall GD of the nth-order quasi-absorptive BPF is given as

$$\tau|_{f=f_0}^{N} = \sum_{i=1}^{N} \tau_i|_{f=f_0}^{\text{Type-I or Type-I}} + = N\,\tau|_{f=f_0}^{\text{Type-I or Type-II}}. \quad (17)$$

To investigate the effect of $2\theta_0$ between one-pole quasi-absorptive BPFs, Fig. 13 shows magnitude/GD responses for the first-order ($n = 1$), second-order ($n = 2$), and

TABLE IV

CIRCUIT PARAMETERS OF THE PROPOSED QUASI-ABSORPTIVE BPFS WITH DIFFERENT FILTER-ORDER AND GD WITH $\theta_0 = 90°$ (REFER TO FIG. 13)

n	Type-I BPF					
	$Z_{0e}(\Omega)$	$Z_{0o}(\Omega)$	$Z_{ot}(\Omega)$	R (Ω)	$\Delta_{GD}(\%)$	$\Delta_{S_{21}-3dB}(\%)$
1	123.27	67.58	50	140	12.45	10.56
2	123.27	67.58	50	140	12.45	7.82
3	123.27	67.58	50	140	12.45	6.40
n	Type-II BPF					
	$Z_{0e}(\Omega)$	$Z_{0o}(\Omega)$	$Z_{ot}(\Omega)$	R (Ω)	$\Delta_{GD}(\%)$	$\Delta_{S_{21}-3dB}(\%)$
1	141.23	81.87	50	110	12.95	10.85
2	141.23	81.87	50	110	12.95	7.84
3	141.23	81.87	50	110	12.95	6.35

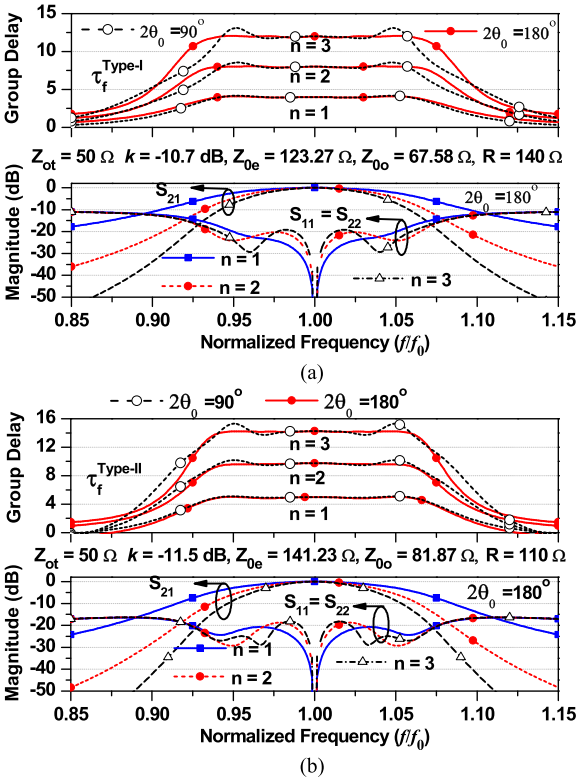

Fig. 13. Magnitude/GD responses of different order ($n = 1$, 2, 3) quasi-absorptive BPFs. (a) Type-I. (b) Type-II.

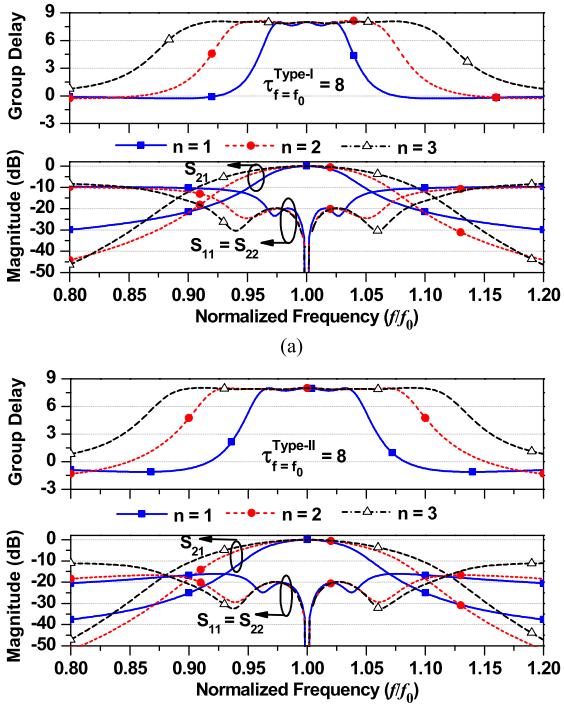

Fig. 14. Magnitude/GD responses of different-order quasi-absorptive BPFs with a fixed maximum GD. (a) Type-I. (b) Type-II.

TABLE V

PROPERTIES CIRCUIT PARAMETERS OF THE PROPOSED QUASI-ABSORPTIVE BPFS WITH DIFFERENT FILTER ORDER, $\tau_{f=f_0} \times f_0 = 8$, AND $2\theta_0 = 180°$ (REFER TO FIG. 14)

n	Type-I BPF					
	$Z_{0e}(\Omega)$	$Z_{0o}(\Omega)$	$Z_{ot}(\Omega)$	R (Ω)	$\Delta_{GD}(\%)$	$\Delta_{S_{21}-3dB}(\%)$
1	128.68	87.29	25	140	5.80	5.60
2	129.63	75.05	50	150	11.20	8.0
3	158.09	85.66	130	310	17.60	10.40
n	Type-II BPF					
	$Z_{0e}(\Omega)$	$Z_{0o}(\Omega)$	$Z_{ot}(\Omega)$	R (Ω)	$\Delta_{GD}(\%)$	$\Delta_{S_{21}-3dB}(\%)$
1	129.62	82.73	25	88	7.60	6.40
2	136.20	71.89	50	101	14.80	8.80
3	163.24	83.77	130	245	20.80	10.80

third-order ($n = 3$) quasi-absorptive BPFs with different θ_0. When $2\theta_0 = 180°$, the ripple in passband GDs is minimum for second- and third-order BPFs. Therefore, we choose $2\theta_0 = 180°$ for designing higher order quasi-absorptive BPF. The calculated circuit parameters, 3-dB passband, and GD FBWs are given in Table IV. As seen from Fig. 13, the in-band GD increased with an increase in the filter-order. With the same circuit parameters, the different-order quasi-absorptive BPFs have increased the GD while maintaining the same in-band GD FBW. In addition, both stopband attenuation and the passband roll-off improved, however, the 3-dB passband FBW decreases accordingly with an increasing number of the filter-order. The input–output return losses are higher than 10 dB for type-I and 15 dB for type-II for all frequencies. Also, all-band quasi-reflectionless behavior can be achieved at both input and output ports.

To demonstrate the in-band GD FBW enhancement capability of the proposed quasi-absorptive BPF, Fig. 14 depicts the S-parameter magnitude and GD responses of the different-order. In these designs, the normalized in-band maximum GD is maintained at a constant value while increasing the filter-order. The circuit parameters are given in Table V. As seen from Fig. 14, the in-band GD and 3-dB FBWs increase with an increase in the filter-order. However, 3-dB passband FBW improvement is relatively smaller as than in-band GD FBW.

Based on these observations, a step-by-step design guideline of the proposed BPFs can be summarized as shown in Fig. 15.

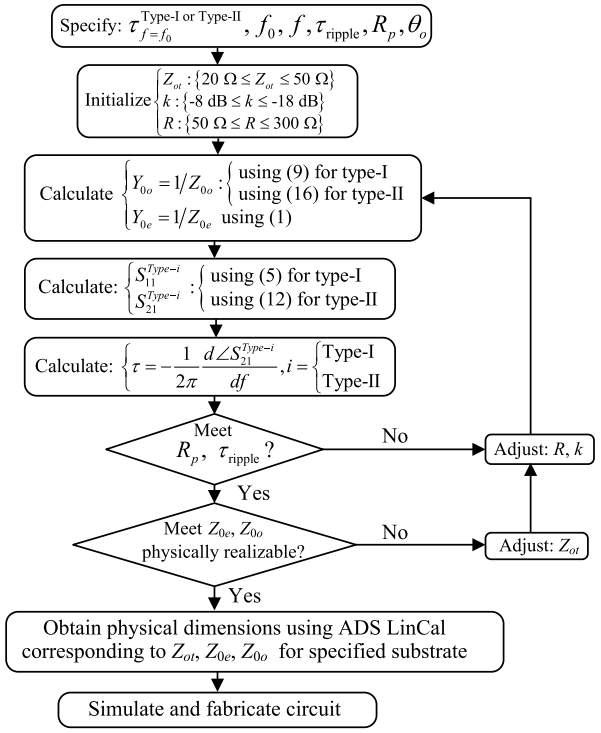

Fig. 15. Design flowchart of the proposed quasi-absorptive BPFs.

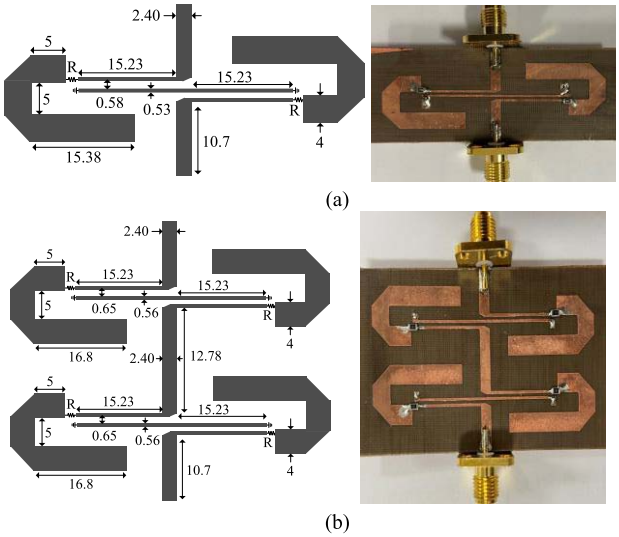

Fig. 16. EM simulation layouts with physical dimensions and photographs of fabricated type-I quasi-absorptive BPFs with prescribed GD. (a) First-order. (b) Second-order. Unit: millimeter (mm).

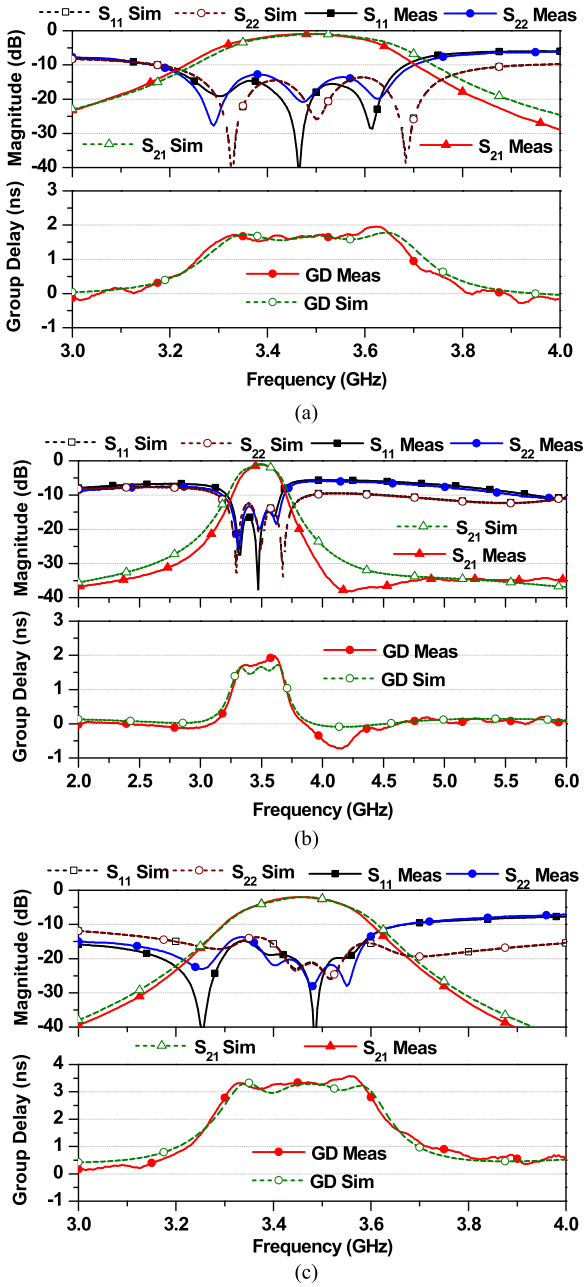

Fig. 17. Magnitude/GD responses of the type-I quasi-absorptive BPFs. (a) First-order narrow-frequency response. (b) First-order wide-frequency response. (c) Second-order narrow-frequency response.

1) The process starts with setting values of $\tau_{f=f_0}^{\text{Type}-i}$, f_0, τ_{ripple}, and maximum reflection in passband R_p where i = type-I or type-II.
2) Once the specifications of BPF are determined, set initial values of Z_{ot}, k, and R. For practical implementation of filter, the values of Z_{ot}, k, and R should be in the range of 20–50 Ω, −8 to −18 dB, and 50–300 Ω, respectively.
3) Determine $Y_{0\text{o}} = 1/Z_{0\text{o}}$ using (8) in case of type-I and using (15) in case of type-II. After obtaining values of $Y_{0\text{o}}$, $Y_{0\text{e}} = 1/Z_{0\text{e}}$ are calculated using (1).
4) After obtaining circuit parameters $Y_{0\text{e}} = 1/Z_{0\text{e}}$, $Y_{0\text{o}} = 1/Z_{0\text{o}}$, and Z_{ot}, calculate S-parameter magnitudes using (6) and (12) for type-I and type-II BPFs, respectively. Using the phase of S_{21}, calculate the GD response according to frequency.
5) Calculate τ_{ripple}, 3-dB passband and GD FBWs using (10) and (11) and compare R_p and τ_{ripple} with the given specifications as shown in step (1). If R_p and τ_{ripple} are not satisfied with the required value, adjust k and R, and then repeat steps (3) and (4).
6) Check physical realizability of $Y_{0\text{e}} = 1/Z_{0\text{e}}$, $Y_{0\text{o}} = 1/Z_{0\text{o}}$. If the coupled line is not realizable practically, then adjust Z_{ot} and repeat steps (3)–(5).

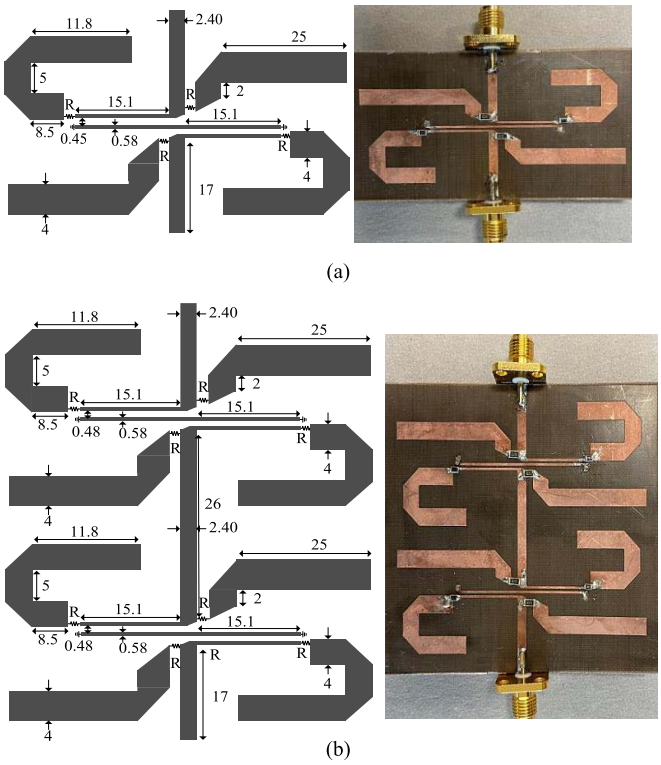

Fig. 18. EM simulation layout with physical dimensions and photographs of fabricated type-II quasi-absorptive BPFs with prescribed GD. (a) $n = 1$. (b) $n = 2$. Unit: millimeter (mm).

7) Higher order BPF can be designed by cascading the first-order BPF.
8) Once all circuit parameters are determined for given specification, obtain physical dimensions of coupled line and TLs, and perform electromagnetic (EM) simulation.

III. Simulation and Experimental Results

For experimental demonstration, the proposed type-I and type-II quasi-absorptive BPFs were designed and fabricated on Taconic substrate with a dielectric constant (ε_r) of 2.20 and thickness (h) of 0.787 mm. The simulation was performed using ANSYS HFSS 2020.

A. Results of the Arbitrarily Prescribed GD Type-I Quasi-Absorptive BPF

The design goal for one-pole equiripple (first-order) type-I BPF is set to $\tau_{f=f_0}^{\text{Type-I}} = 1.75$ ns at $f_0 = 3.50$ GHz with maximum passband reflection $R_p = 15$ dB and $\theta_0 = 45°$. Using the design procedures outlined in Fig. 15, the calculated circuit parameters of the first-order quasi-absorptive BPF ($n = 1$) for given specifications are determined as $Z_{\text{ot}} = 35\ \Omega$, $R = 130\ \Omega$, $k = -12.6$ dB, $Z_{0\text{e}} = 147.8333\ \Omega$, and $Z_{0\text{o}} = 91.6848\ \Omega$. For experimental validation, open-circuited $\lambda/2$ stub is chosen instead of short-circuited $\lambda/4$ stub because of lower characteristic impedance needed for the later one which makes it is not feasible. Fig. 16(a) shows the layout with the physical dimensions and photograph of the fabricated BPF.

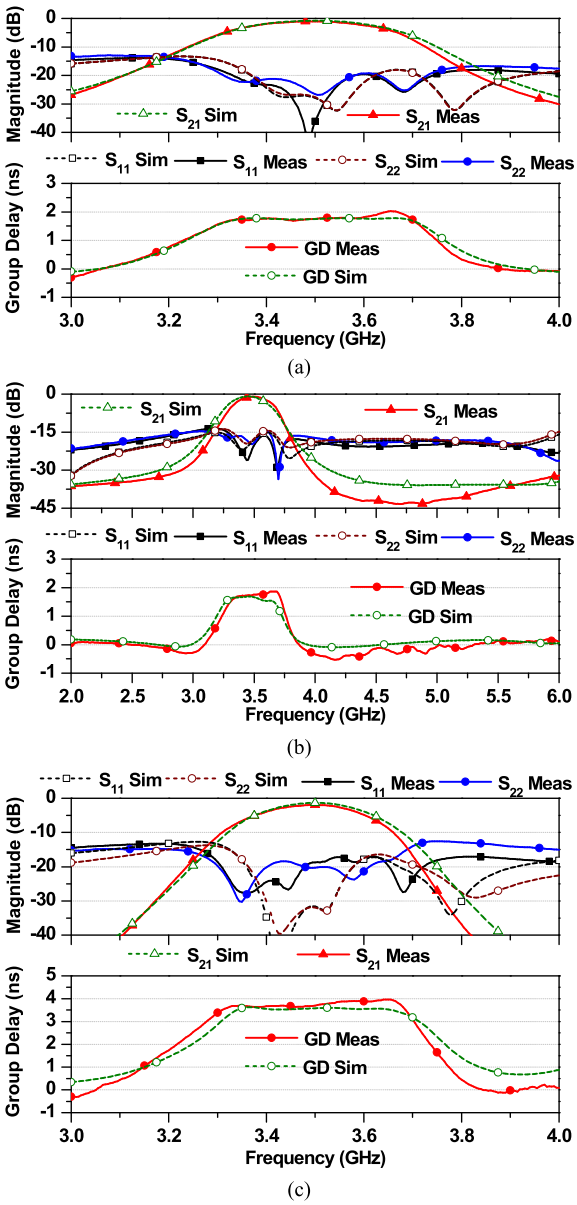

Fig. 19. Magnitude/GD response of type-II quasi-absorptive BPFs. (a) First-order narrow-frequency response. (b) First-order wideband-frequency response. (c) Second-order narrow-frequency response.

Fig. 17(a) shows the simulated and measured GDs and S-parameter magnitudes of the first-order type-I quasi-absorptive BPF. The measurement results agree well with the simulation. The measured GD and IL at $f_0 = 3.50$ GHz are 1.72 ns and 0.91 dB, respectively. The measured GD and 3-dB passband FBWs are 10.28% (3.305–3.665GHz) and 8.71% (3.32–3.63 GHz), respectively, with GD variation of 1.65–1.92 ns. Similarly, the measured input–output return losses are higher than 18.05 dB/17.65 dB at $f = f_0$ and higher than 6 dB at all frequencies.

Fig. 16(b) shows the layout and fabricated circuit photograph of the second-order quasi-absorptive BPF with prescribed GD. The circuit parameters for the second-order designed BPF are the same as those of first-order. The simulated and measured GDs and S-parameter magnitudes of

TABLE VI
PERFORMANCE COMPARISON OF THE PROPOSED BPFS WITH STATE-OF-ARTS

	f_0 (GHz)	IL (dB)	RL (dB)	$\tau_{f=f_0}$ (ns)	Δ_{GD} (%)	$\Delta_{S_{21}-3dB}$ (%)	A	Circuit Size
[14]	1	0.91	16.5/11	x	x	8.80	No	$0.47\lambda_g \times 0.23\lambda_g$
[17]	3.86	1.8	15/9.7	x	x	9.30	No	NA
[25]	3.0	1.20	18/10	x	x	11	No	$1.14\lambda_g \times 0.50\lambda_g$
[26]	2.45	2.20	14.8/20	4	6	6	No	$1.25\lambda_g \times 0.42\lambda_g$
[27]	2.45	0.60	18/13	1.10*	x	22.5	No	$0.71\lambda_g \times 0.46\lambda_g$
This work^{I}	**3.50**	**0.91**	**18/10**	**1.72**	**10.28**	**8.71**	**Yes**	$\mathbf{0.28\lambda_g \times 0.70\lambda_g}$
This work^{II}	**3.50**	**2.10**	**25/9.5**	**3.40**	**7.72**	**5.80**	**Yes**	$\mathbf{0.44\lambda_g \times 0.70\lambda_g}$
This work^{III}	**3.50**	**1.03**	**26.6/14**	**1.76**	**11.71**	**9**	**Yes**	$\mathbf{0.42\lambda_g \times 0.80\lambda_g}$
This work^{IV}	**3.50**	**1.96**	**18/14**	**3.70**	**11.06**	**6.72**	**Yes**	$\mathbf{0.76\lambda_g \times 0.80\lambda_g}$

A: arbitrarily prescribed group delay capability
RL: input/output return losses at f_0/all frequencies
*: simulated group delay using ideal circuit parameters [27]

second-order BPF are shown in Fig. 17(b). The measured GD and IL at $f_0 = 3.50$ GHz are determined as 3.40 ns and 2.10 dB, respectively. The measured GD varies from 3.20 to 3.56 ns with in-band GD and 3-dB passband FBWs of 7.72% and 5.8%, respectively. Similarly, the input–output return losses are higher than 25 dB at f_0 and higher than 8 dB in all frequencies.

B. Results of Arbitrarily Prescribed GD Type-II Quasi-Absorptive BPF

The type-II quasi-absorptive BPF was designed and fabricated at $f_0 = 3.50$ GHz with $\tau_{f=f_0}^{\text{Type-II}} = 1.75$ ns. The calculated optimum circuit parameters of the first-order type-II quasi-absorptive BPF for the given specification are given as $\theta_0 = 45^\circ$, $Z_{\text{ot}} = 35\ \Omega$, $k = -12$ dB, $R = 100\ \Omega$, $Z_{0\text{e}} = 139.3290\ \Omega$, and $Z_{0\text{o}} = 83.3856\ \Omega$. In this design example, open-circuited $\lambda/2$ stub is chosen instead of short-circuited $\lambda/4$ stub because of lower characteristic impedance. Fig. 18(a) shows the layout and photograph of the fabricated type-II circuit.

Fig. 19(a) shows the measured and simulated S-parameter magnitudes and GDs. These results show that the measurement results are in good agreement with the simulation and theoretical predicated values.

From the experiment, the GD is 1.76 ns at f_0 and the passband flat GD extends from 3.30 to 3.71 GHz. The flat in-band GD and 3-dB passband FBWs of the fabricated first-order type-II filter are given as 11.71% and 9%, respectively, which is slightly wider than the type-I BPF for a similar GD. Similarly, the measured S-parameters at $f_0 = 3.50$ GHz are determined as $|S_{21}| = -1.04$ dB, $|S_{11}| = -36.15$ dB and $|S_{22}| = -26.60$ dB, and measured input–output return losses are higher than 14 dB for all frequencies.

For the experimental validation of a higher order BPF, Fig. 18(b) presents the layout and photograph of the second-order type-II BPF. The circuit parameters are the same as the first-order BPF. Fig. 19(b) shows the measured and simulated S-parameter magnitudes and GDs of the second-order type-II BPF. The measured GD and IL at $f_0 = 3.50$ GHz are determined to be 3.70 ns and 1.96 dB, respectively. The measured passband GD varies from 3.50 to 3.96 ns with an FBW of 11.06% (3.295–3.682 GHz). Similarly, the measured 3-dB passband FBW of fabricated filter is determined to be 6.72%, which is smaller than in-band GD FBW. Similarly, the input–output return losses at f_0 are determined to be 15.65/15.50 dB, respectively. The input–output return losses are higher than 13.4 dB in all frequencies. A performance comparison of the proposed BPFs with state-of-arts is shown in Table VI. As seen from Table VI, the proposed BPF provides a quasi-absorptive filter response with an arbitrarily prescribed flat GD. In addition, the proposed BPF structures are very simple and can be easily extended to higher orders for a high GD or enhanced GD bandwidth.

IV. CONCLUSION

This work demonstrates novel microstrip line absorptive BPFs with arbitrarily prescribed GD response. The proposed filters can achieve a two-port quasi-absorptive response over a wide frequency range. To achieve absorption at all frequencies, the absorptive stubs consisting of a series resistor and short-circuited quarter-wavelength stub or open-circuited half-wavelength stubs are connected at coupled lines. The absorptive sections not only eliminate out-of-band reflections, but also play an important role in achieving the passband flat GD response. Higher order absorptive BPFs with an arbitrarily prescribed GD can be easily designed by cascading the first-order symmetrical quasi-absorptive BPFs. The experimental validation of the proposed filter design methodology was conducted by designing, fabricating, and measuring a set of quasi-absorptive filters with arbitrarily prescribed GD and various orders.

REFERENCES

[1] B. Mini-Circuits, "Reflectionless filters improve linearity and dynamic range," *Microw. J.*, vol. 58, no. 8, pp. 42–50, Aug. 2015.
[2] C. Caloz, S. Gupta, Q. Zhang, and B. Nikfal, "Analog signal processing: A possible alternative or complement to dominantly digital radio schemes," *IEEE Microw. Mag.*, vol. 14, no. 6, pp. 87–103, Sep. 2013.
[3] K. E. Kolodziej and J. G. McMichael, "Multitap RF canceller for in-band full duplex wireless communications," *IEEE Trans. Wireless Commun.*, vol. 15, p. 6, pp. 4321–4334, Jun. 2016.

[4] Y. Jeong, D. Ahn, C. D. Kim, and I. S. Chang, "A feed-forward amplifier using an equal group delay signal cancellation technique," *Microw. J.*, vol. 50, no. 4, pp. 126–134, Apr. 2007.
[5] N. Aaron Estep, D. L. Sounas, and A. Alù, "Magnetless microwave circulators based on spatiotemporally modulated rings of coupled resonators," *IEEE Trans. Microw. Theory Techn.*, vol. 64, no. 2, pp. 502–518, Feb. 2016.
[6] Y. Yu *et al.*, "Radio frequency magnet-free circulators based on spatiotemporal modulation of surface acoustic wave filters," *IEEE Trans. Microw. Theory Techn.*, vol. 67, no. 12, pp. 4773–4782, Dec. 2019.
[7] G. Chaudhary and Y. Jeong, "Arbitrary prescribed wideband flat group delay circuits using coupled lines," *IEEE Trans. Microw. Theory Techn.*, vol. 66, no. 4, pp. 1885–1894, Apr. 2018.
[8] A. C. Guyette, I. C. Hunter, and R. D. Pollard, "Design of absorptive microwave filters using allpass networks in a parallel-cascade configuration," in *IEEE MTT-S Int. Microw. Symp. Dig.*, Jun. 2009, pp. 733–736.
[9] M. A. Morgan and T. A. Boyd, "Theoretical and experimental study of a new class of reflectionless filter," *IEEE Trans. Microw. Theory Techn.*, vol. 59, no. 5, pp. 1214–1221, May 2011.
[10] M. A. Morgan and T. A. Boyd, "Reflectionless filter structures," *IEEE Trans. Microw. Theory Techn.*, vol. 63, no. 4, pp. 1263–1271, Apr. 2015.
[11] C. Jackson, "Transmission line replacements for a lumped element reflectionless filter," in *Proc. IEEE Radio Wireless Symp. (RWS)*, San Diego, CA, USA, Jan. 2014, pp. 166–168.
[12] C. M. Jackson, "Reflectionless filters for miniaturized space applications," in *Proc. IEEE Topical Workshop Internet Space (TWIOS)*, Jan. 2018, pp. 20–23.
[13] T.-H. Lee, B. Lee, and J. Lee, "First-order reflectionless lumped-element lowpass filter (LPF) and bandpass filter (BPF) design," in *IEEE MTT-S Int. Microw. Symp. Dig.*, May 2016, pp. 1–4.
[14] D. Psychogiou and R. Gomez-Garcia, "Reflectionless adaptive RF filters: Bandpass, bandstop, and cascade designs," *IEEE Trans. Microw. Theory Techn.*, vol. 65, no. 11, pp. 4593–4605, Nov. 2017.
[15] D. J. Simpson, R. Gomez-Garcia, and D. Psychogiou, "Mixed-technology quasi-reflectionless planar bandpass filters," in *Proc. 48th Eur. Microw. Conf. (EuMC)*, Sep. 2018, pp. 551–554.
[16] M. Khalaj-Amirhosseini and M.-M. Taskhiri, "Twofold reflectionless filters of inverse-chebyshev response with arbitrary attenuation," *IEEE Trans. Microw. Theory Techn.*, vol. 65, no. 11, pp. 4616–4620, Nov. 2017.
[17] R. Gomez-Garcia, J.-M. Munoz-Ferreras, and D. Psychogiou, "Split-type input-reflectionless multiband filters," *IEEE Microw. Wireless Compon. Lett.*, vol. 28, no. 11, pp. 981–983, Nov. 2018.
[18] R. Gomez-Garcia, J.-M. Munoz-Ferreras, and D. Psychogiou, "RF reflectionless filtering power dividers," *IEEE Trans. Circuits Syst. II, Exp. Briefs*, vol. 66, no. 6, pp. 933–937, Jun. 2019.
[19] R. Gomez-Garcia, J.-M. Munoz-Ferreras, and D. Psychogiou, "Symmetrical quasi-reflectionless BSFs," *IEEE Microw. Wireless Compon. Lett.*, vol. 28, no. 4, pp. 302–304, Apr. 2018.
[20] R. Gomez-Garcia, J.-M. Munoz-Ferreras, W. Feng, and D. Psychogiou, "Balanced symmetrical quasi-reflectionless single-and dual-band bandpass planar filters," *IEEE Microw. Wireless Compon. Lett.*, vol. 28, no. 9, pp. 798–800, Sep. 2018.
[21] J. Lee, T. C. Lee, and W. J. Chappell, "Lumped-element realization of absorptive bandstop filter with anomalously high spectral isolation," *IEEE Trans. Microw. Theory Techn.*, vol. 60, no. 8, pp. 2424–2430, Aug. 2012.
[22] J.-Y. Shao and Y.-S. Lin, "Narrowband coupled-line bandstop filter with absorptive stopband," *IEEE Trans. Microw. Theory Techn.*, vol. 63, no. 10, pp. 3469–3478, Oct. 2015.
[23] M. Kong, Y. Wu, Z. Zhuang, Y. Liu, and A. A. Kishk, "Compact wideband reflective/absorptive bandstop filter with multi transmission zeros," *IEEE Trans. Microw. Theory Techn.*, vol. 67, no. 2, pp. 482–493, Feb. 2019.
[24] A. C. Guyette, I. C. Hunter, R. D. Pollard, and D. R. Jachowski, "Perfectly-matched bandstop filters using lossy resonators," in *IEEE MTT-S Int. Microw. Symp. Dig.*, 2005, pp. 516–520.
[25] S.-W. Jeong, T.-H. Lee, and J. Lee, "Absorptive filter prototype and distributed-element absorptive bandpass filter," in *IEEE MTT-S Int. Microw. Symp. Dig.*, Aug. 2018, pp. 1–4.
[26] R. Gomez-Garcia, J.-M. Munoz-Ferreras, and D. Psychogiou, "Symmetrical quasi-absorptive RF bandpass filters," *IEEE Trans. Microw. Theory Techn.*, vol. 67, no. 4, pp. 1472–1482, Apr. 2019.
[27] X. Wu, Y. Li, and X. Liu, "High-order dual-port quasi-absorptive microstrip coupled-line bandpass filters," *IEEE Trans. Microw. Theory Techn.*, vol. 68, no. 4, pp. 1462–1475, Apr. 2020.

Girdhari Chaudhary (Member, IEEE) received the B.E. degree in electronics and communication engineering from Nepal Engineering College (NEC), Kathmandu, Nepal, in 2004, the M.Tech. degree in electronics and communication engineering from MNIT, Jaipur, India, in 2007, and the Ph.D. degree in electronics engineering from Jeonbuk National University, Jeonju, South Korea, in 2013.

He is currently working as an Assistant Research Professor with the Division of Electronics Engineering, Jeonbuk National University. He worked as a Principal Investigator (PI) of independent project through Basic Science Research Program of the National Research Foundation (NRF) of Korea funded by the Ministry of Education Korea. His research interests include multiband tunable passive circuits, in-band full duplex systems and high-efficiency power amplifiers, negative group delay circuits, and its applications.

Dr. Chaudhary was a recipient of the BK21 PLUS Research Excellence Award 2015 from the Ministry of Education, South Korea. He has received Korean Research Fellowship (KRF) through the National Research Foundation (NRF) of Korea funded by the Ministry of Science and ICT. He has served as a reviewer for IEEE TRANSACTIONS ON MICROWAVE THEORY AND TECHNIQUES, IEEE MICROWAVE AND WIRELESS COMPONENTS LETTERS, IEEE TRANSACTIONS ON CIRCUITS AND SYSTEMS I: REGULAR PAPERS, and IEEE TRANSACTIONS ON INDUSTRIAL ELECTRONICS.

Yongchae Jeong (Senior Member, IEEE) received the B.S.E.E., M.S.E.E., and Ph.D. degrees in electronics engineering from Sogang University, Seoul, South Korea, in 1989, 1991, and 1996, respectively.

From 1991 to 1998, he worked as a Senior Engineer with Samsung Electronics, Seoul, Republic of Korea. In 1998, he joined the Division of Electronics Engineering, Jeonbuk National University, Jeonju, South Korea. From July 2006 to December 2007, he was a Visiting Professor with the Georgia Institute of Technology, Atlanta, GA, USA. He had also served as the Director of the HOPE-IT Human Resource Development Center of BK21 PLUS, Jeonbuk National University, where he is currently a Professor and also a member of the IT Convergence Research Center. He is currently teaching and conducting research in microwave passive and active circuits, mobile and satellite base-station RF system, design of periodic defected transmission line (TL), negative group delay circuits and its applications, in-band full duplex radio, and RFIC design. He has authored or coauthored over 250 articles in international journals and conference proceedings.

Prof. Jeong is a member of the Korea Institute of Electromagnetic Engineering and Science (KIEES).